Implementation and Analysis of a Digital Model of the Incremental-Quantity Distance Element Using EMTP

Toby Russell, Prashanna Bhattarai, and Mickey Cox, *Louisiana Tech University*
Milton Quinteros and Thomas Field, *Entergy Services LLC.*

***Abstract*— This paper discusses the governing principles and overall design of the incremental-quantity distance element present in commercially available time-domain-based protective relays (TDRs), as well as the details pertaining to the digital implementation of this element using the Electromagnetic Transients Program (EMTP). Analysis of the performance of this element under various fault scenarios is presented as well. It also discusses the limitations of the model, along with some of the assumptions that were made during its implementation in EMTP. The model is validated using a commercially available TDR by utilizing the event-playback testing capabilities of these modern relays. This new capability is utilized not only in the performance analysis testing, but also in the core functionality design of the digital model. The principal advantage of this modern time-domain-based approach to power system protection is the speed at which the protection elements can operate after a fault is sensed on a transmission line. The rapid operating time gives this protection technique a competitive edge over traditional phasor-domain impedance-based protection schemes from which these modern techniques are derived.**

***Index Terms*— traveling waves, incremental quantity, distance element, line-protection relay, and electromagnetic transients.**

I. Introduction

TRADITIONAL phasor-based protective elements have minimum operating times of approximately one cycle after a fault for most cases, and can be as short as half a cycle for best-case scenarios [1]. The operating speed of these elements is mainly limited by the time required to accurately measure the new faulted state phasors [1]. In contrast, the incremental-quantity (IQ) distance element (TD21) present in the new time-domain-based relays (TDRs) can operate within a few milliseconds [2] after detecting the fault. Such a rapid operation is made possible because the TD21 element's algorithm is based on the instantaneous quantities, and is not limited by phasor calculations and communication delays [3].

Even though the TD21 element utilizes the line impedance values in its algorithm, its governing principles are quite separate from those utilized in the traditional impedance- and admittance-based protective relays such as the impedance-type, modified impedance-type, reactance-type, or the mho-type distance relays. These traditional methods, also referred to as phasor-based protection elements, operate strictly by relying on the phasors measured at the relay terminals. In contrast, the TD21 element is based in the time domain and utilizes the superposition principles to extract the IQs which represent the change in the system following a fault.

Since the TDRs are based on a relatively new technology, detailed analysis of their performance, especially by end users or independent researchers, are not in abundance. Even though [4], [5] discuss the operational characteristics of TDRs, neither the digital simulation models nor discussions of detailed modeling and design of the constituent elements of TDRs, including the TD21, are readily available in literature.

This paper discusses in detail the design and digital implementation of the TD21 element using the electromagnetic transients program (EMTP). Published literature that discuss the fundamentals of this model [1], [3], [5], [6] are used as the primary reference, while real-world commercially available TDRs are used for the model validation.

Several assumptions had to be made during the modeling of the element due to the sparsity of available information as well as the limitations of the software package used in the modeling. One of these limitations pertains to the down-sampling of input data. Real world TDRs sample the raw data at the rate of 1 MHz and then the data is down-sampled at 10 kHz for use in the IQ-based elements [6]. To mimic this operation, a down-sampling method was developed where the system simulations were performed using a step-size that corresponds to sampling rate of 1 MHz and the data was then exported into a separate file, consisting of the distance element relay model signal processing, where the simulations were performed using a step-size that corresponds to the sampling rate of 10 kHz. However, the results indicated that the element performed basically the same regardless of down-sampling, except for points very close to the reach point where the higher resolution signal processing generated slightly larger or smaller operating signal magnitudes which lead to operational discrepancies in marginal cases. Therefore, down-sampling was not included in the final design of the element because the added complexity did not yield proportional improvement in accuracy. Next, the internal low pass filter was estimated to have a cutoff frequency of about 125 Hz, and some of the thresholds and scaling factors were estimated by using available documentation and comparing against TDR test results. These nuances are discussed in detail in the later sections of this paper. Although the design of the digital model is not identical to that of the TDRs due to these assumptions, the model nonetheless mimics the operation of the TD21 element of the TDRs for the majority of the cases tested.

The primary objective of this paper is to provide insight in-

to the digital implementation and design process of the IQ distance element available in ultra-high-speed TDRs. The model discussed herein can be used in transient studies of systems and fault events to help predict the operation of TDRs in the field under various operating conditions.

II. Overview of Governing Principles

A. Application of the Superposition Principle in Fault Analysis

Superposition principle is used in the analysis of faulted networks to separate the prefault and the fault-induced quantities. Consider the prefault network depicted in Fig. 1 consisting of two sources and a defined fault location where the fault point voltage can be determined [7].

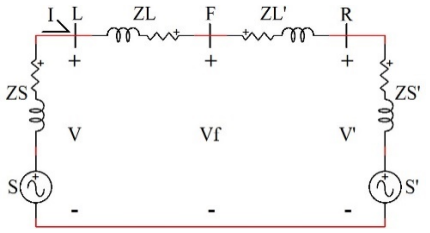

Fig. 1. Prefault network circuit

Next, to represent the fault generated network, a similar circuit is designed with the terminal sources short-circuited. In this circuit, a new source is added at the point of the fault with a voltage that is equal but opposite to the prefault voltage at that point [7]. This fault-generated network has only one source at the fault point in addition to any impedances given in the prefault configuration. The fault circuit is shown in Fig. 2.

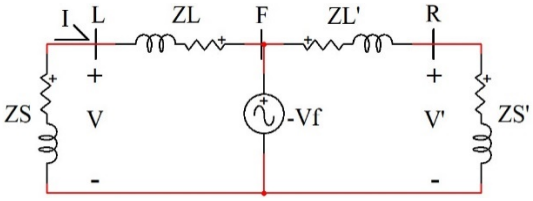

Fig. 2. Fault-generated network circuit.

The prefault and fault-generated circuits are analyzed separately to determine the prefault and the fault induced components, the sum of which is the postfault or faulted network depicted in Fig. 3 [1].

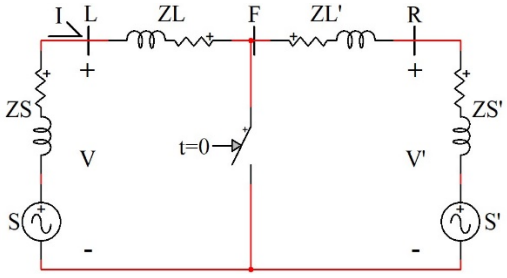

Fig. 3. Postfault network circuit.

The superposition principle is an important tool in fault analysis because it provides a method of breaking up a fault event into three separate independent circuits. This paper will focus on the prefault and the fault generated circuits for the development of the governing equations. The voltages and currents observed in the fault-generated network are known as the IQs; they represent the change in conditions from steady-state to postfault and are typically denoted with a "Δ" in the script, as shown in Eq. (1)-(7). These change-in-state conditions are typically calculated by subtracting a quantity's value during the previous cycle, which represents the prefault steady-state condition, from the present or postfault values [3]. The IQs are extracted using a base-delta filter shown in Fig. 4 in its block diagram form. The input to the filter is the instantaneous voltage or current signal measured by the instrument transformers. The delay block implements a one-power-cycle delay, and the output is the difference between the instantaneous and the delayed values. When the system is under steady-state conditions, the output of the base-delta filter will be approximately zero because the voltages and currents should not have changed in the duration of one cycle [2].

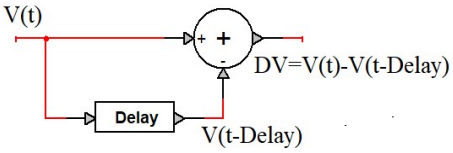

Fig. 4. Base-delta filter block diagram.

If the system is faulted, the output of the filter will represent the change in conditions referenced as the faulted network for exactly one cycle duration following a fault. These IQ values will only be valid for one cycle after the fault because once this window is exceeded, the one-cycle-old data no longer represents the prefault steady-state conditions of the circuit. The output of the base-delta filter contains only the transients generated by the fault, and does not include the prefault steady-state values [1].

B. IQ Distance Element Operating Principles

IQ distance elements can operate at high speeds because they are based on calculations from signals observed in real-time along with the signals recorded from the previous cycle. They do not require the additional filter delays associated with phasor calculations. Therefore, once the simple signal processing, which includes a short filter delay, is completed, the element can operate immediately, assuming the necessary conditions are met. This element has a settable reach point, and it should only trip for faults within the set reach. It operates by calculating the steady-state and the incremental voltages at the set reach point with current and voltage signals measured at the relay terminals [3]. The element uses a restraining voltage calculated using the prefault voltage at the reach point as an input. The incremental signal calculated at the reach point provides an output that represents the magnitude of change due to the fault, and this signal is called the operating voltage or operating signal. Next, the operating and the restraining signals are compared against one another, which provides the basis for the trip decision. The EMTP model discussed herein also differs slightly from the physical TDRs relays while making the trip decision. In the model, if the magnitude of the operating signal exceeds that of the re-

straining signal and they are of opposite polarity, then the fault is deemed to be within the reach point, thereby causing the element to operate. As such, there is no additional security margin. However, in the physical relays, the difference between the two signals are added together for a short window using an accumulator, and the element will operate if the output of the accumulator exceeds a pre-defined threshold [3]. The reason for not including the accumulator in the model is because some of the necessary information about it is proprietary and could not be gathered. As a result of this, the model slightly over-reaches compared to the physical relays. To account for this, yet another variable, referred to as the *restraining signal scaling factor* [1], was adjusted in the model to negate the differences arising due to the lack of the accumulator. The scaling factor is discussed in more detail in IV.

Given a fault at the reach point, the condition that causes the largest incremental signal occurs when the voltage drops to zero due to a bolted fault [5]. As fault impedance is added, the magnitude of the reach point voltage decreases in an inverse relationship with fault impedance [2]. This relationship will cause the incremental-quantity distance element to underreach proportionally with the fault impedance until the fault impedance reaches a point where the change given by the incremental signal will never exceed the value of the restraining signal [2]. Therefore, like traditional distance elements, this element is not always dependable during fault scenarios involving large fault impedances.

The voltage at the reach point is calculated for six fault types, namely, *Phase-A-to-ground, Phase-B-to-ground, Phase-C-to-ground, Phase-A-to-B, Phase-B-to-C,* and *Phase-C-to-A*. For each fault type, the independent fault loop is derived where the voltage at the reach point is calculated. This voltage is calculated with both the incremental current and voltage signals as well as with the one-cycle-old steady-state voltage and current signals. These fault loop equations are derived from the general fault network circuit shown in Fig. 2. These impedances are scaled by the reach point setting that is a percentage of the protected line to determine the voltage at this location.

First a line-to-ground fault loop is considered. This is accomplished by using a combination of Thevenin's theorem for two-port networks and the superposition principle to solve the faulted network [1]. The circuit shown in Fig. 5 is used to derive the loop equations for the Phase-A fault loop.

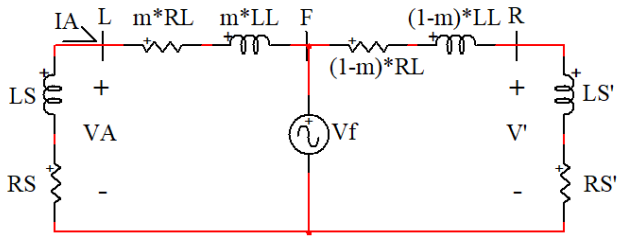

Fig. 5. Phase A fault loop circuit.

The circuit depicted in Fig. 5 is a modified version of the fault-generated network circuit given earlier in Fig. 2 with specific elements that can be related to known or measured values in the protected power system. Both the operating and restraining signals are derived from the same circuit with the only difference being that the restraining signal uses one-cycle-old voltage and current signals measured at the relay and the operating signal uses incremental voltage and current signals generated using the delta filter depicted earlier in Fig. 4.

In the Phase-A fault loop circuit given in Fig. 5, the VA and IA values are the instrument transformer voltage and current readings from the relay terminals respectively, while 'L' and 'R' indicate the local and the remote terminals, respectively. The reach setting is denoted by 'm'. This circuit is designed to find the voltage at the set reach point by multiplying the reach with the line impedance between the fault and the local relay terminal. It can be assumed that the line impedance is a complex value with both nonzero R and L components. Circuit theory is applied to the loop circuit and expressions for the loop replica current and incremental loop replica current are derived resulting in the flowing equations (the 1 and the 0 subscripts denote the positive and the negative sequences, respectively):

$$I_{ZA} = \left[b_1 \cdot I_A + b_2 \cdot \frac{dI_A}{dt}\right] + \left[b_3 \cdot I_o + b_4 \cdot \frac{dI_o}{dt}\right] \quad (1)$$

and,

$$\Delta I_{ZA} = \left[b_1 \cdot \Delta I_A + b_2 \cdot \frac{d\Delta I_A}{dt}\right] + \left[b_3 \cdot \Delta I_o + b_4 \cdot \frac{d\Delta I_o}{dt}\right] \quad (2)$$

where the following constants are declared to simplify the equations above:

$$b_1 = \frac{R_1}{|Z_1|}, b_2 = \frac{L_1}{|Z_1|}, b_3 = \left(\frac{R_o - R_1}{|Z_1|}\right), b_4 = \left(\frac{L_o - L_1}{|Z_1|}\right) \quad (3)$$

Using the above relations, the expressions for the restraining (V_{rst}) and the operating (V_{op}) signals can be derived:

$$V_{rst} = V_{AG} - \left(b_1 \cdot I_A + b_2 \cdot \frac{dI_A}{dt} + b_3 \cdot I_o + b_4 \cdot \frac{dI_o}{dt}\right) \cdot m \cdot |Z_1| \quad (4)$$

and,

$$V_{op} = \Delta V_{AG} - \left(b_1 + \Delta I_A + b_2 \cdot \frac{d\Delta I_A}{dt} + b_3 \cdot \Delta I_o + b_4 \cdot \frac{d\Delta I_o}{dt}\right) \cdot m \cdot |Z_1| \quad (5)$$

These relationships are the same for all three line-to-ground loops. The line-to-line fault loops are derived in a similar manner with the primary difference being that none of the zero sequence components are used. The relationships for the line-to-line restraining and operating voltages are:

$$V_{rst} = V_{AB} - \left[b_1 \cdot I_{AB} + b_2 \cdot \frac{dI_{AB}}{dt}\right] \cdot m \cdot |Z_1| \quad (6)$$

and,

$$V_{op} = \Delta V_{AB} - \left[b_1 \cdot \Delta I_{AB} + b_2 \cdot \frac{d\Delta I_{AB}}{dt}\right] \cdot m \cdot |Z_1| \quad (7)$$

III. Event Playback Testing Procedure for the SEL-T400L Time-Domain Line Protection Relay

A. Event Playback Testing

Event playback testing is a modern approach to testing time-domain-based ultra-high-speed relays and the feature is available in the SEL-T400L Time-Domain Line Protection relay (to be referred to as the SEL-T400L Relay), the TDR used in this study. In this method, event files generated using electromagnetic transient simulation programs can be played back to the relays, and, as such, it enables relay testing without the need for test equipment. The principal advantage to this type of testing is that an accurate representation of the high

frequency transient behavior of a faulted system can be applied to the devices under test without bandwidth limitations.

To complete playback testing,

- a suitable test file that contains an accurately modeled power system must be available in an electromagnetic transient study program.
- This file must be configured with appropriately rated voltage and current transformers so that the secondary voltage and current signals have magnitudes within the specified range of the intended relay under test.
- Additionally, this file must be configured to run at a step-size of one microsecond or smaller, and the overall file length must be between 0.1 s and 24 s in duration [3].
- Next, a fault scenario is simulated using the system model.
- After the simulation, the three-phase voltage and current secondary signals must be stored in a COMTRADE file format. Each signal should be given a unique name that properly identifies the individual signals such as: IA, IB, IC, VA, VB, and VC.
- Next, all voltage and current signals that are to be applied to the relay under test must be saved as a single COMTRADE file. This file is given a unique name so that it can be identified throughout the test procedure and located if additional testing is required.
- After the file(s) have been generated, they must be converted to a file format that can be accepted and loaded on the TDRs [8].
- Once converted to the appropriate format the resulting file can be loaded on the relay under test and the test can be initiated.

A detailed synopsis of the relay's operation can be observed by downloading the event files generated by the relays after each test case is completed. The test procedure is discussed in more detail in [9].

B. Event Playback Testing Applications

Event playback testing is utilized in the design as well as the verification of the digital model discussed herein. As stated previously, the TDR used in this study has a time-domain IQ distance element referred to as the TD21 [3], which is the basis of the digital model implemented in this paper. Through playback testing, the operation of the TD21 element in the TDR can be examined and recorded under specific fault conditions. Additionally, the digital model can also be tested under identical faulted conditions. Then, the results can be compared, and necessary modifications can be made to the digital model, so that its response mimics that of the TDR's TD21 element as closely as possible. In addition, unit-step signal can be applied to the TDRs through playback testing methods to analyze the filtering elements within the relays.

IV. Development of the Incremental-Quantity Distance Element Digital Model

The development of the digital model of the IQ distance element using EMTP is discussed in this section. The digital model is also validated using a TDR at each major step. Although the model was designed to mimic the final operation of the TD21 element in the TDR, the individual blocks and signal processing techniques that are presented are not identical to the TD21 elements in the TDR. In other words, while the final operation of the model and the TD21 elements are similar in nature, the design of the blocks is not identical.

A. Initial Settings

Global variables can be configured in EMTP with what is called a mask by introducing them at the top level of each subcircuit. The mask is where the element's settings are entered. The TD21 element in the TDR requires the positive- and the zero-sequence line impedances along with the line length and reach settings. These same settings are entered using the same units into the mask of the digital model. Additionally, a few constants and threshold variables are also declared in the mask to simplify the design and tuning of the element. One such variable is the restraining signal scaling factor or "Vrst_SF" which is a small margin added to the restraining signal for added security [3]. This scaling factor is said to be some value greater than one to provide an additional security margin [1]. Using playback testing and a trial-and-error approach, this scaling factor was determined to be 1.06 for the digital model. The authors discovered that the scaling factor used in the TDR was 1, but it was adjusted and fine-tuned to be greater than 1 in the digital model to account for the lack of the accumulator discussed earlier in the paper.

B. Model Overview

The approach taken in the design of the digital model was to organize tasks in a logical manner where similar blocks were lumped together in smaller subcircuit blocks allowing for simplified troubleshooting and ease of use. The first layer of the element is depicted in Fig. 6. Each of the constituent blocks are discussed in the subsequent sections in more detail.

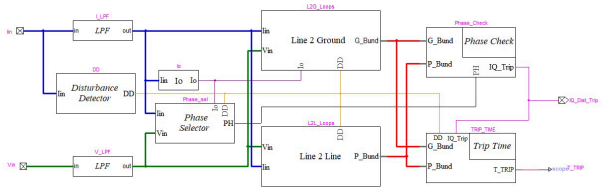

Fig. 6. Distance element top level subcircuit.

C. Filter Design

The TD21 element relies on a low-pass anti-aliasing filter that removes the high-frequency content present in the incoming current and voltage signals from the instrument transformers [5]. As a result of having this filter, the frequency spectrum of the TDR's TD21 element is in the range of a few hundred hertz [3]. The filter of the digital model was designed using MATLAB and then implemented using EMTP. Event reporting and playback testing features of the TDRs were utilized extensively during the filter design process. Many signals are available in event files that can be downloaded from the relays following a test that leads to a trip outcome. The extracted signals in these files come from various points in the signal processing chain, and some can be utilized in the design of certain elements within the model. One such signal is simply the filtered response to an input voltage waveform. It is esti-

mated that the only processing applied to this signal is the internal anti-aliasing filter along with the element's low-pass filter. Therefore, with careful manipulation of the input test file, a simple unit-step input can be disguised as a voltage signal, loaded on the TDRs, and run through the filters to observe the step response in the event files. The filter's step response is provided in Fig. 7. The step response characteristics such as the rise time and percent overshoot were measured and recorded. The readers will notice that the magnitude of the input in the step-response shown in Fig. 7 is not 1V. This is because the signal processing present in the relays attenuates the input signal to some extent. As a result, even when a unit-step input is applied to the relays, the actual input that gets applied to the TDRs low-pass filter (LPF) is close to 0.6V. In addition, the filter in the TDR gets automatically turned off after approximately 20 milliseconds, leading to the response as depicted by the green trace in Fig. 7.

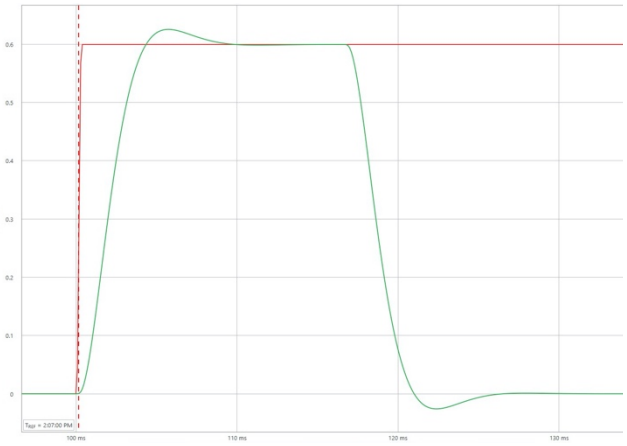

Fig. 7. Step-response of the SEL-T400L Relay's internal lowpass filter.

While designing the filter for the incremental-quantity distance element, the assumption was made that the internal low-pass filter in the TDR was likely a low-order filter. Beginning with low-order Butterworth and Chebyshev low-pass filters, a trial-and-error approach was applied to try and mimic the step response characteristics of the TDR's internal low-pass filter. It was observed that the frequency spectrum of the TDR's TD21 element was of the order of a few hundred hertz [3]. This insinuates that the cutoff frequency of the low-pass filter is likely in the range of 100 to 300 Hz. The filter was initially designed using MATLAB and then implemented in EMTP after it had been validated. The step response of the filter designed using MATLAB is provided in Fig. 8. As shown in Fig. 8, the overshoot and the rise time of the filter designed in MATLAB are very close to that of the internal low-pass filter inside the TDR depicted in Fig. 7. Additionally, it was observed in both responses that just after the initial overshoot, the filter output has a small undershoot below unity for a short duration (not to be confused with the undershoot below 0 after the filter is the turned off in Fig. 7). MATLAB provided a transfer function that was easily implemented in EMTP in the *LPF* block in Fig. 6. The unit-step response of the LPF in EMTP is shown in Fig. 9. The input was turned off after 20 milliseconds to better resemble the operation in the TDR.

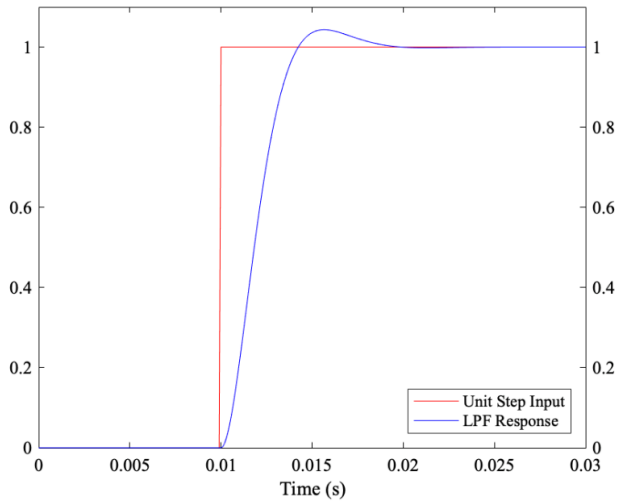

Fig. 8. Unit-step-response of the lowpass filter designed using MATLAB.

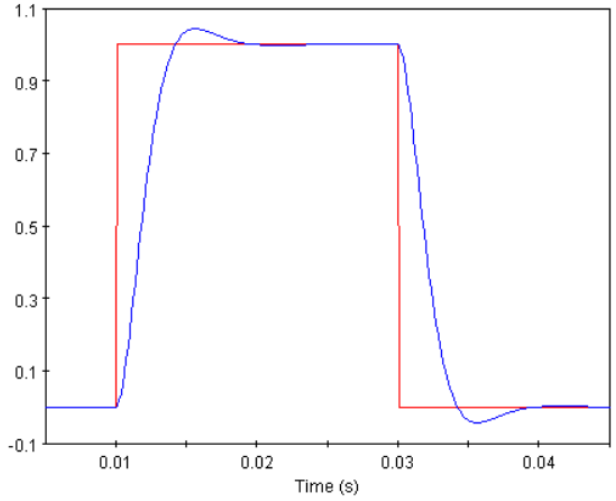

Fig. 9. Unit-step-response of the lowpass filter implemented in EMTP.

D. Disturbance Detector

The disturbance detector (DD) used for the digital model's design is very simple and sensitive. It will pick up faults on the protected system very quickly and provide an output that transitions from zero to one after a disturbance. It will remain on for one cycle before resetting to zero. This output is a prerequisite for the trip logic in the TD21 element to operate and the one cycle duration prevents the element from operating more than one cycle post fault because by that point the incremental signals are no longer a valid representation of the fault induced changes.

E. Line-to-Ground Fault Loop Logic

All calculations for the line-to-ground fault loops happen in the "Line 2 Ground" block of the block diagram depicted in Fig. 6. The subcircuit of the this block is shown in Fig. 10. As shown, each individual line-to-ground fault loop block receives the filtered current (blue) and voltage (green) signals respective to its phase. Each block receives the DD output as

well as the zero-sequence current. The zero-sequence current is only used for the line-to-ground calculations, and it is calculated only once in the "Io" block as shown in Fig. 6.

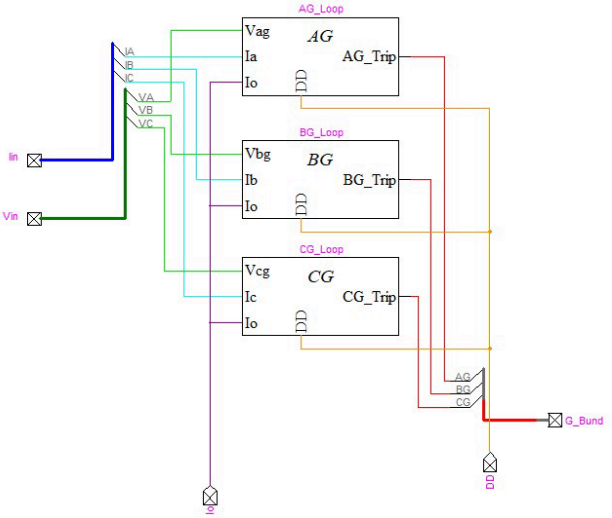

Fig. 10. Subcircuit of the Line 2 Ground block.

The subcircuit of each of the three fault loops shown in Fig. 10, namely *AG*, *BG*, and *CG*, are identical, and are shown in Fig. 11. This is where the base or raw operating and restraining voltages are calculated for each fault loop.

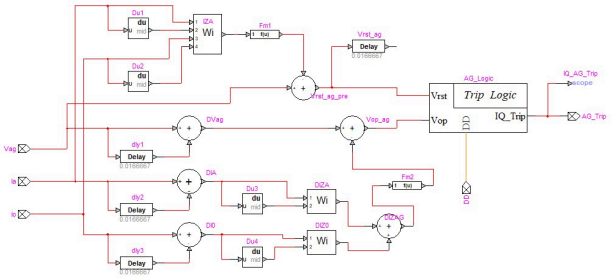

Fig. 11. Individual LG fault loop subcircuit.

The restraining signal is calculated in the "Vrst_ag" blocks which are shown at the top of the diagram. Equation (4) is implemented in EMTP in this section of the block. To do so, the derivative of the filtered current signals is first calculated, and the scaling factors are applied in the weighted sum block denoted by "IZA" in block diagram in Fig. 11. Next the loop replica current "IZA" is multiplied by the reach setting and the positive sequence line impedance magnitude. Finally, this product is subtracted from the filtered phase voltage. The output of this block is the pre-restraining signal. The operating signal is calculated based on the incremental quantity values. This is done by subtracting exactly one cycle old data from the current cycle data to represent the change in the faulted network.

F. Trip Logic

The raw operating signal and the pre-restraining signal are passed into the "Trip Logic" block. This block is the same for all fault loops and the subcircuit is shown in Fig. 12.

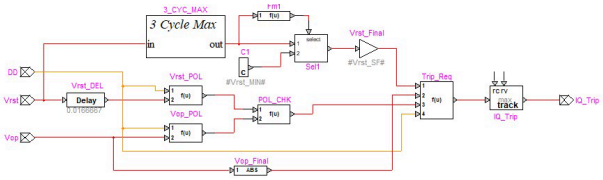

Fig. 12. Subcircuit of the Trip Logic block.

The incremental-quantity distance element requires that the raw operating and restraining signals be of opposite polarities for trip requirements to be met. In addition, the digital model requires the DD supervision to be active. Therefore, none of the blocks will operate unless the DD output is high. The "Vrst_POL" and "Vop_POL" blocks require that DD and the input signal be greater than zero to operate. As such, the output of these blocks is high only if the input signal is in the positive region of the cycle. The next block is "POL_CHK" which provides an output of one only if the inputs are of opposite polarities.

The next step is to derive the final restraining signal. This process starts with the pre-restraining signal that has yet to be delayed. It is explained in [5] that the final restraining signal consists of the "sub-cycle-max" of three signals: one that is exactly one cycle old, another that is slightly before that one-cycle-old data, and finally one that is slightly after the exact one-cycle-old data. Reference [5] depicts a final restraining signal that has a flat-topped shape that appears the be a slightly elongated version of the original restraining signal. Using this figure and other figures in [5] that depict real fault scenarios, it was estimated that the time between the sub-cycles is roughly 0.6667 ms. This is implemented using the "*3 Cycle Max*" block shown in Fig. 12. The waveforms obtained using this block are depicted in Fig. 13 where the three traces on the top plot are the sub-cycle waveforms, while the trace in the bottom plot is the maximum instantaneous value of these three waveforms.

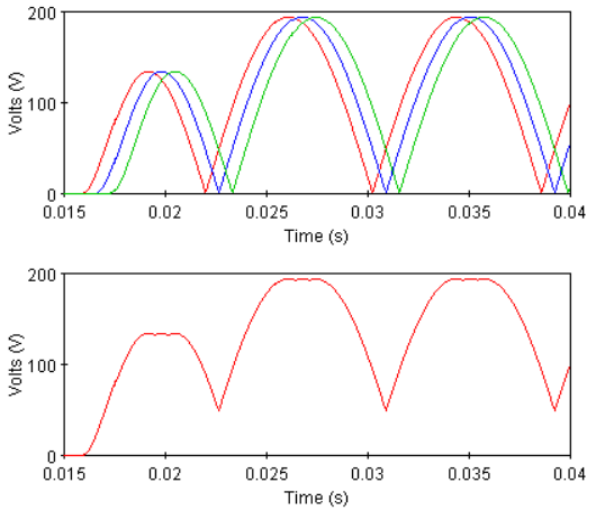

Fig. 13. Operation of the 3 Cycle Max block: top plot depicting the one-cycle-old (blue), sub-cycle delayed (red), and sub-cycle advanced (red) waveforms, and the bottom plot depicting the maximum instantaneous value of these three waveforms.

The next step in finding the final restraining signal is implementing a minimum restraining level, called "Vrst_MIN", to protect against false tripping near a zero-crossing [5]. As before, using figures in [5] that depict real fault scenarios, a good estimate for the minimum restraining level was found to be roughly 50 Volts. This is implemented in the next set of blocks in EMTP using an output selector block. If the input is 50 Volts or greater, the output will reflect the value of the input. However, if the input is less than 50 Volts, the output will remain at 50. Finally, the output is scaled by the scaling factor "Vrst_SF" discussed earlier to produce the final restraining signal which is depicted in Fig. 14 in blue. The raw restraining signal in red is also provided for reference.

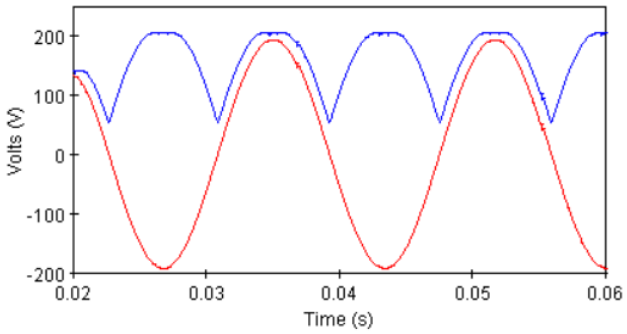

Fig. 14. Comparisons between the raw (red) and the final (blue) restraining signals.

G. Line-to-Line Fault Loop Logic

The line-to-line fault loops are implemented in a similar nature to the line-to-ground loops with the main difference being that the zero-sequence currents are not used.

H. Phase Selector

The incremental-quantity distance element has six loops (one for each of the three line-to-ground and the three line-to-line faults) that can trip for a given fault scenario. Therefore, the model blocks must determine the fault type and verify that the correct loop operates when intended. The operating signal measures the change from the steady-state operation to its postfault scenario. This signal stays at or near zero until a fault occurs, after which its value represents the change in magnitude from steady state to postfault. In theory, this magnitude will be the largest in the faulted loop. The loop selector for the incremental-quantity distance element selects the faulted loop by choosing the loop with the operating signal that has the largest peak magnitude during the first postfault cycle [1].

I. Phase Check

The incremental-quantity distance element must check to ensure that the loop correlating to the selected fault type indicated by the phase selector operates with the incremental quantity logic. This step occurs in the "Phase Check" Circuit block in the block diagram shown in Fig. 6. The model will check to ensure that the appropriate loop has operated, and if so, it will generate a high output. Next, a logic block is implemented that provides a final output of zero for cases without any fault and an output of -1 if the faulted loop did not meet the incremental-quantity distance element's trip requirements. This will occur for faults that are either in the reverse direction or beyond the reach point in the forward direction.

J. Trip Time

The "Trip Time" block, shown in the bottom right section of the block diagram in Fig. 6, provides an output that indicates the time duration between when the disturbance detector detected a fault on the line until the instant when the trip requirements are met on the appropriate faulted loop. Although its EMTP subsystem is not shown in this paper, it simply tracks the outputs of the DD block and the TD21 bit and calculates the time difference between their respective assertion.

V. Model Validation

A. Test System Used for Model Validation

Testing the incremental-quantity distance element requires a model that is representative of a typical power system in which the protection element is applied. Modeling such a system requires accurate information about the sources, loads, transmission lines, and instrument transformers. Since the incremental-quantity distance element relies on prefault current and voltage signals, the system must also have sufficient load that draws the necessary prefault current. Additionally, the positive- and the zero-sequence line impedance values must be available to be applied to the settings of the distance element blocks. The system used for the testing is depicted in Fig. 15. It consists of two synchronous machines and constant parameter lines. The protected line is 175 km long and is connected to the synchronous machines via external lines, 150 km in length, at each end. The relays and the instrument transformers are placed at each end of the protected line.

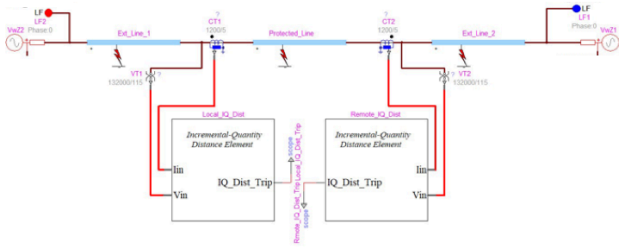

Fig. 15. Test system.

The protected line system settings are shown in TABLE 1:

TABLE 1
TEST SYSTEM SETTINGS

System voltage level	230 kV
VT Ratio	132000 / 115
CT Ratio	1200 / 5
Per-length positive-sequence impedance of all lines (at 60 Hz)	$(0.02+j0.339)\ \Omega/km$
Per-length zero-sequence impedance of all lines (at 60 Hz)	$(0.3+j\ 0.113)\ \Omega/km$

B. Summary of Test Plan

After configuring the system and the appropriate settings, the basic operation of the model is tested by running preliminary simulations and ensuring that the element is tripping

when it absolutely should, and not tripping when it should not. We know that the model should not operate during external faults; it should operate for faults on the protected line that occur very close to the respective terminal, and this operation region should extend out to roughly the reach point. However, the reach point is not an exact specification of the element's reach; due to the system specific parameters, fault inception angle, and the security measures included in the design, the distance elements will typically trip to within 5 to 10 percent of the reach point setting [5]. This means that the operation of the elements can become less predictable and might vary slightly from system to system around the reach point.

After ensuring that the element is fully secured and generally dependable, the next step is to fine-tune the value of the restraining voltage scaling factor. This is done by first playing back a set of test cases on the TDRs and recording the operation of the TD21 element for each. Since the most profound differences will only be observed around the reach point, all of these simulations are completed for faults near the theoretical reach point location. Additionally, a variety of fault types are used for these simulations to ensure that different scenarios are considered, and operational differences due to fault inception angles are mitigated. Once the tests have been completed with the TDRs, the same tests are again completed with the EMTP distance element blocks. The "Vrst_SF" is adjusted until the block has close agreement with the TDRs.

C. Preliminary EMTP Simulation Results

In the preliminary testing, the reach is set to 0.7 for both line-to-line and line-to-ground fault loops, which equals to approximately 122.5 km. Simulation results are depicted in TABLE 2 which indicate that the element's operation was fully secured, and generally dependable. Neither the local nor the remote relay operated during any of the external fault cases (presented in the first two and the last two rows of the table). As the fault location was moved into the protected line, the appropriate element began tripping for faults that occurred within the reach point. In addition, as the fault approached the reach point, the elements became less dependable.

Fig. 16 shows the raw operating (red trace) and restraining (blue trace) signals for a close-in C-to-A fault located 1 km from the local terminal on the protected line. The depicted raw restraining signal that is delayed by one cycle but not yet scaled by the scaling factor and without the sub-cycle max signal processing. Note that they are of opposite polarity for the first cycle after the fault.

Fig. 17 shows the final operating and restraining signals for the same CA fault for both the local (top plot) and the remote (bottom plot) relays. These final operating and restraining signals only depict the magnitudes of the respective signals. The final operating signal is simply the absolute value of the raw operating signal, but as described above, the final restraining signal undergoes some modifications. These signals are used to determine whether the operating signal exceeds the restraining signal, and thereby the trip decision. If the final operating signal exceeds the final restraining signal, and, if the raw signals are of opposite polarities, then the TD21 digital model element will operate.

TABLE 2
PRELIMINARY SIMULATION RESULTS USING THE IQ DISTANCE ELEMENT DIGITAL MODEL IMPLEMENTED IN EMTP

Fault introduced at 0.099 seconds				
Line Length (km)	**Fault Distance from Local Relay (km)**	**Fault Type**	**I.Q. Distance Element Local**	**I.Q. Distance Element Remote**
175	**-10**	CG	NT	NT
	-5	AB	NT	NT
	1	AG	TRIP	NT
	1	CA	TRIP	NT
	20	CG	TRIP	NT
	20	AB	TRIP	NT
	25	BG	TRIP	NT
	25	BC	TRIP	NT
	75	AG	TRIP	TRIP
	75	AB	TRIP	TRIP
	95	BG	TRIP	TRIP
	95	CA	TRIP	TRIP
	120	CG	NT	TRIP
	120	BC	NT	TRIP
	135	AG	NT	TRIP
	135	BC	NT	TRIP
	145	CG	NT	TRIP
	145	CA	NT	TRIP
	173	BG	NT	TRIP
	173	AB	NT	TRIP
	178	CG	NT	NT
	181	AB	NT	NT

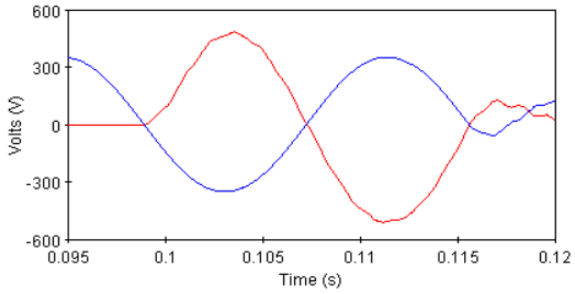

Fig. 16. Raw restraining (blue) and operating (red) signals for a close-in fault.

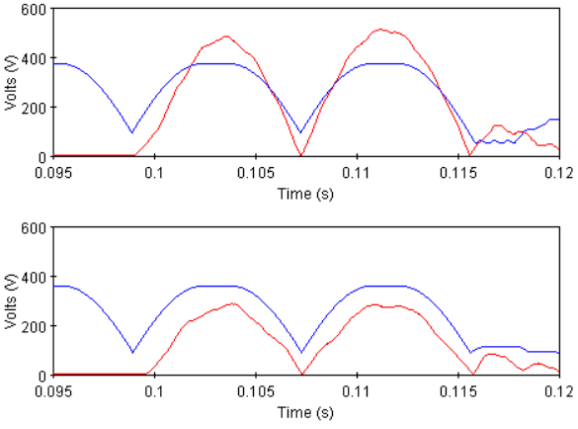

Fig. 17. Final operating (red) and restraining (blue) signals calculated at the local (top) and the remote (bottom) relays for a close-in CA fault 1 km away from the local terminal.

Note how the final operating signal (red traces) in Fig. 17 no longer retains its form after one full cycle postfault as this delayed signal begins to show the effects of the fault. Once this signal begins to degrade, the logic is no longer valid, and the supervision will prevent the element from operating.

If a fault is located towards the center of the line, then the distance element at both terminals should operate. In this scenario, the operating signals at both relay terminals should have similar magnitudes. In addition, the line impedance seen from each end to the fault location should also be roughly the same.

Fig. 18 shows the final operating (red trace) and restraining (blue trace) signals for a fault roughly located near the center of the protected line (90 km from the local terminal and 85 km from the remote terminal) for both the local (top plot) and the remote (bottom plot) relays.

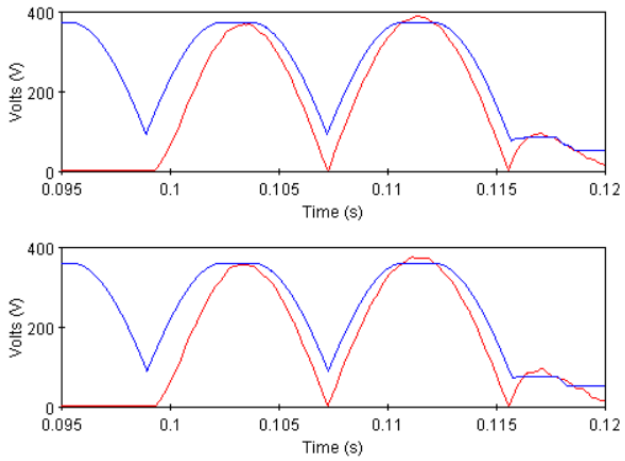

Fig. 18. Final operating (red) and restraining (blue) signals calculated at the local (top) and the remote (bottom) relays for a fault located approximately half-way along the protected line.

Observing Fig. 18, it is evident that the trip requirements were not met at either of the relays until the second peak of the operating signal. It was generally observed for the cases tested in this paper that when the fault is located farther away from the relay terminals or near the reach point, the distance element typically operates on the second peak of the operating signal. On the other hand, it was also observed that for test cases where the fault is located near the relay terminal, the trip conditions are usually met during the first peak of the restraining signal like the top plot in Fig. 17. However, it is important to note that the cases tested herein were only for bolted faults. Presence of fault resistance tends to attenuate the incremental quantities, making the fault seem further down the line. For such cases, trip requirements might not be met until the second peak, if at all, even for close-in faults, leading to a longer operating time. Therefore, it can be deduced that the operating time of the element is likely to increase with the increase in both the distance to fault, as well as the fault resistance. Furthermore, the fault inception angle also tends to impact the element's operating time to some extent.

D. Comparisons with the TDR Test Results

The first set of simulations of this category, provided in TABLE 3, were run on the TDRs to establish a baseline for the TD21 element's operation. These tests were only run for cases that are close to the reach point since the main purpose of these simulations was to determine the scaling factor used for the final restraining signal. After the simulations were completed on the TDRs, similar tests were run on the EMTP relay model shown in the right-side columns of TABLE 3. Starting at 1.01, the scaling factor (K) was increased until the operation of the digital model was in close agreement with that of the TDRs for most of the cases. As this scaling factor is increased, the actual reach is slightly reduced compared to the ideal reach setting. The inclusion of this scaling factor increases the magnitude of the restraining signal which in turn requires a larger operating signal to produce a trip scenario, thereby decreasing the reach of the element as the scaling factor is increased.

TABLE 3
COMPARISON OF RESULTS BETWEEN THE DIGITAL MODEL AND THE SEL-T400L RELAY FOR DIFFERENT FAULT TYPES

Incremental Quantity Distance Element Comparison						
Fault Introduced at 0.099 seconds						
Line Length (km)	Fault Distance from Local Relay (km)	Fault Type	T400L Relays		EMTP Model (K=1.06)	
			TD21 Local	TD21 Remote	I.Q. Distance Element Local	I.Q. Distance Element Remote
175	66	AG	TRIP	NT	TRIP	NT
	66	BC	TRIP	NT	TRIP	NT
	67	CG	TRIP	NT	TRIP	NT
	67	AB	TRIP	TRIP	TRIP	TRIP
	68	BG	TRIP	TRIP	TRIP	NT
	68	CA	TRIP	NT	TRIP	NT
	69	CG	TRIP	TRIP	TRIP	TRIP
	69	AB	TRIP	TRIP	TRIP	TRIP
	70	BG	TRIP	TRIP	TRIP	TRIP
	70	BC	TRIP	TRIP	TRIP	TRIP
	98	CG	TRIP	TRIP	TRIP	TRIP
	98	AB	TRIP	TRIP	TRIP	TRIP
	99	BG	TRIP	TRIP	NT	TRIP
	99	AB	TRIP	TRIP	TRIP	TRIP
	100	AG	NT	TRIP	NT	TRIP
	100	BC	NT	TRIP	NT	TRIP

Observing the results TABLE 3, there were only two test cases in which the TDRs and the digital model disagreed with one another (indicated in red). These were for two different phase B-to-ground faults, located 99 km and 68 km away respectively from the local relay terminal. The final operating and restraining signals were observed, and it was determined that for both these cases, the magnitude difference that caused the non-trip case was less than half-a-volt. Since the difference was small, it was deduced that a very small discrepancy in the scaling factor could be causing the differences observed in the distance elements operation near the reach point. In addition, the discrepancies could also be partially attributed to the fact that the TDR down-samples the input data to 10 kHz for the TD21 calculations, whereas such down-sampling does not take place on the digital model as explained earlier. Based on prior simulations, it was determined that the digital model operates very well when sampled at 1 MHz, but the addition of down-sampling can cause small differences in signal magnitudes resulting in operational differences for marginal cases that are very close to the reach point.

A significant underreach (below set reach setting) of the TD21 element was noted in TABLE 3. This was attributed to the combination of the element's design [5] and the operating conditions (the lengths of the external lines, for example). To

verify this, simulations were run by changing the length of the two external lines in the system shown in Fig. 15, referred to as the *original test system* for clarity, from 150 km to 10 km. This increased the reach of the TD21 element by approximately 4%. However, since the underreach below the set reach point seen in the results obtained using the *original test system* was seen in the model as well as the TDRs physical relays, and the focus of the paper was just on the digital implementation of the element, it was concluded that the *original test system* was adequate to verify the accuracy of the digital implementation. As such, the *original test system*, consisting of the 150 km external lines on each side of the protected line depicted in Fig. 15, was used for the additional simulations. Nonetheless, results suggest that the increase in source-to-impedance ratio tends to cause the element to underreach.

The discrepancies between the digital model and the TDRs during the phase BG fault cases were further investigated. Tests were completed at 1 km increments to determine the differences in the trip range for the BG fault cases. The results of these additional simulations are shown in TABLE 4.

TABLE 4
COMPARISON OF RESULTS BETWEEN THE DIGITAL MODEL AND THE SEL-T400L RELAY DURING BG FAULTS AT VARYING FAULT LOCATIONS

Incremental Quantity Distance Element Comparison						
Fault Introduced at 0.099 seconds						
Line Length (km)	Fault Type	Fault Distance from Local Relay (km)	T400L Relays		EMTP Model (K=1.06)	
			TD21 Local	TD21 Remote	I.Q. Distance Element Local	I.Q. Distance Element Remote
175	BG	64	TRIP	NT	TRIP	NT
		65	TRIP	NT	TRIP	NT
		66	TRIP	TRIP	TRIP	NT
		67	TRIP	TRIP	TRIP	NT
		68	TRIP	TRIP	TRIP	NT
		69	TRIP	TRIP	TRIP	TRIP
		70	TRIP	TRIP	TRIP	TRIP
		96	TRIP	TRIP	TRIP	TRIP
		97	TRIP	TRIP	TRIP	TRIP
		98	TRIP	TRIP	NT	TRIP
		99	TRIP	TRIP	NT	TRIP
		100	TRIP	TRIP	NT	TRIP
		101	TRIP	TRIP	NT	TRIP
		102	TRIP	TRIP	NT	TRIP
		103	TRIP	TRIP	NT	TRIP
		104	NT	TRIP	NT	TRIP
		105	NT	TRIP	NT	TRIP
		106	NT	TRIP	NT	TRIP

It is apparent from the results shown in Table 4 that the TD21 element in the TDRs tripped for a slightly larger range of values than the digital model. The tests were completed again with the scaling factor K reduced to 1.05 which yielded results that had a closer agreement with the TDRs for BG faults; however, this reduced scaling factor caused a larger number of disagreements between the model and the TDRs for other tests cases shown in TABLE 3. More attempts were made at tuning the scaling factor to get complete agreement between the model and physical relays, but this goal was never achieved. It was therefore decided that adjusting the scaling factor K, denoted by "Vrst_SF" in the digital model, does cause small differences in the operation of the digital model, but since it is not the only difference between the model and the TDRs, it cannot be adjusted to get perfect agreement. The results indicate that the optimal value of the scaling factor in the digital model is 1.06 in its present stage. Therefore, the scaling factor was set to that value.

VI. Conclusion

A digital model of an incremental-quantity distance element developed using the Electromagnetic Transients Program (EMTP) software package was presented in this paper. The design was based on the TD21 element in the SEL-T400L Relays developed by Schweitzer Engineering Laboratories. The TD21 is an underreaching protective element with no intentional time delay that does not require communication with the remote relay. The developed model was also validated using the SEL-T400L Relay. The event playback testing capability of the SEL-T400L Relay was utilized extensively during the validation and testing of the model. While there were certain design discrepancies between the digital model and the physical relays, the digital model closely mimicked the operation of the physical relays. Both the model and the physical relays operated correctly for all close-in faults on the protected line and did not operate for any external faults. The element operated within a few milliseconds of fault detection for most fault cases; however, as the distance to the fault increased, the operating times did increase slightly. There were certain operational discrepancies between the relay and the model, which were more pronounced during fault scenarios near the reach point setting of the element. In these situations, the difference between tripping or not tripping is often due to a very small margin in the operating signal magnitude, which is likely due to the discrepancies between the signal processing in the computer model and the SEL-T400L Relays. Overall, the EMTP incremental-quantity distance element performed well for most scenarios as a fast and secure high-speed protection element.

Although time-domain-based relays consisting of the incremental quantity distance element are becoming increasingly common in the power transmission system, detailed digital models of these elements are not readily available yet in electromagnetic transient analysis software packages. The final operation of the digital model discussed herein closely tracks that of the commercially available relay, and, as such, can be utilized in transient studies to predict the behavior of the TD21 element of the relays in the field.

VII. Acknowledgment

The authors would like to thank Entergy for funding the project. Authors would also like to thank Schweitzer Engineering Laboratory for providing two state-of-the-art SEL-T400L Time-Domain Line Protection Relays to Louisiana Tech University for the project. Authors would also like to acknowledge the support from Mr. Jeremy Blair and Mr. Mihajlo Curcic during the project.

VIII. References

[1] E. O. Schweitzer, B. Kasztenny, A. Guzman, V. Skendzic, and M. V. Mynam, "Speed of line protection - can we break free of phasor limitations?," in *2015 68th Annual Conference for Protective Relay Engineers*, College Station, TX, USA, Mar. 2015, pp. 448–461. doi: 10.1109/CPRE.2015.7102184.

[2] G. Benmouyal, N. Fischer, and B. Smyth, "Performance comparison between Mho elements and incremental quantity-based distance elements," in *2017 70th Annual Conference for Protective Relay Engineers (CPRE)*, College Station, TX, Apr. 2017, pp. 1–19. doi: 10.1109/CPRE.2017.8090043.
[3] Schweitzer Engineering Laboratories, "SEL-T400L Ultra-High-Speed Transmission Line Relay Traveling-Wave Fault Locator High-Resolution Event Recorder, Instruction Manual." Schweitzer Engineering Laboratories, 2018. [Online]. Available: http://selinc.com
[4] J. P. G. Ribeiro and F. V. Lopes, "Modelling and simulation of a time-domain line protection relay," *J. Eng.*, vol. 2018, no. 15, pp. 861–865, Oct. 2018, doi: 10.1049/joe.2018.0272.
[5] E. O. Schweitzer, B. Kasztenny, and M. V. Mynam, "Performance of time-domain line protection elements on real-world faults," in *2016 69th Annual Conference for Protective Relay Engineers (CPRE)*, College Station, TX, USA, Apr. 2016, pp. 1–17. doi: 10.1109/CPRE.2016.7914904.
[6] Schweitzer Engineering Laboratories, "SEL-T401L Ultra-High-Speed Line Relay - Instruction Manual." Schweitzer Engineering Laboratories, Jan. 2021. [Online]. Available: https://selinc.com
[7] M. Vitins, "A Fundamental Concept for High Speed Relaying," *IEEE Trans. Power Appar. Syst.*, vol. PAS-100, no. 1, pp. 163–173, Jan. 1981, doi: 10.1109/TPAS.1981.316873.
[8] P. A. Crossley and P. G. McLaren, "Distance Protection Based on Travelling Waves," *IEEE Trans. Power Appar. Syst.*, vol. PAS-102, no. 9, pp. 2971–2983, Sep. 1983, doi: 10.1109/TPAS.1983.318102.
[9] L. M. Wedepohl, "Application of matrix methods to the solution of travelling-wave phenomena in polyphase systems," *Proc. Inst. Electr. Eng.*, vol. 110, no. 12, p. 2200, 1963, doi: 10.1049/piee.1963.0314.
[10] E. Clarke, *Circuit Analysis of A-C Power Systems*. General Electric, Schenectady, NY, 1950.
[11] Hermann W. Dommel, *Electromagnetic Transients Program (EMTP) Theory Book*. Bonneville Power Administration, Portland, OR, 1987.

IX. Biographies

Toby Russell Toby Russell attended Louisiana Tech University where he earned a Master's degree in Electrical Engineering in November of 2021 and a Bachelor's degree in Electrical Engineering with an emphasis on power and control systems in May 2020. His senior capstone project focused on the design and construction of a megohmmeter insulation tester that was capable of generating a test voltage of 500 volts DC and measuring resistances in the megaohm range. His graduate research was conducted under the supervision of Dr. Prashanna Bhattarai and Dr. Mickey Cox, and focused on power system protection, specifically focusing on the modeling and testing of traveling wave relays and performing transient studies using the EMTP software package. He has several years of experience using various system and transient analysis software, as well as hands-on experience using state-of-the-art power protection hardware. Toby also has more than 10 years of in-the-field experience installing and troubleshooting access controls systems.

Prashanna Bhattarai (M'2016) earned a BS degree in electrical engineering from Tribhuvan University - Pulchowk Campus, Kathmandu, Nepal, in 2008, and the MS and PhD degrees in electrical engineering from Louisiana State University, USA, in 2013 and 2016 respectively. He is currently an Assistant Professor of Electrical Engineering in the College of Engineering and Science at Louisiana Tech University. His was previously employed as a lecturer of electrical engineering at Louisiana Tech University, graduate assistant at Louisiana State University, and graduate student intern at Entergy. His research interests include power system protection, power system modeling and transients, electric machines, and power quality. He is a member of IEEE.

Mickey D. Cox (SM'88) received the B.S. and M.S. degrees from Louisiana Tech University, Ruston, in 1976 and 1978 and the Ph.D. degree from Louisiana State University, Baton Rouge, in 1986. From 1978 to 1980 he was an Aerosystems Engineer, analyzing and designing antennas with the General Dynamics Corporation, Fort Worth, TX. He served for 39 years as a faculty member in electrical engineering at Louisiana Tech University and upon his retirement in 2022 he was designated Professor Emeritus. He is a Registered Professional Engineer in the State of Louisiana. His current research interests include electrical machinery and power system protection.

Milton Quinteros received a Bachelor of Science in Electrical Engineering in May 2007, and his Master of Science in Electrical Engineering in May 2009 from the University of New Orleans. He finished working on his Doctoral degree at the same University in December 2014. He is currently working in Entergy Services Inc. as Sr. Engineer in the Standards and Design Group. His research areas include Digital Telecommunications, Data Base design, Digital, and Communications for Power System Protection and Automation. Dr. Quinteros is a member of IEEE since 2007, member of Eta Kappa Nu chapter Iota Rho, and member of Tau Beta Pi Epsilon chapter since 2012.

Thomas Field received a BSEE from the University of New Orleans in 1988 and a MSEE in power from Louisiana State University in 1993. After graduating from LSU, he worked for Nashville Electric Service performing EMTP studies in the Relay and Communications group until 1998, ComEd performing real time transient simulator studies until 1999, Southern Company performing EMTP studies until 2004, and WAPA in the Desert Southwest transmission planning group until 2007. He is currently a Senior Staff Engineer at Entergy where he is responsible for the real time transient simulator lab and university research projects. He is a senior member of IEEE PES, IAS, and SA. He has been a member of several IEEE standards working groups and is currently past chair of the IEEE Mississippi Section.